applied sciences

MDPI

Article

Height Control System for Wind Turbines Based on Critical Wind Speed Calculation

Alina Fazylova [1,2], Teodor Iliev [3,*], Ivaylo Stoyanov [4] and Eduard Siemens [5]

[1] Department of Electronic Engineering, Almaty University of Power Engineering and Telecommunications Named After G.Daukeev, Almaty 050013, Kazakhstan; a.fazylova@aues.kz
[2] Department of Transport Construction and Production of Building Materials, LB Goncharov Kazakh Automobile and Road Institute, pr. Rayymbeka, 417, Almaty 050061, Kazakhstan
[3] Department of Telecommunications, University of Ruse, 8 Studentska Str., 7004 Ruse, Bulgaria
[4] Department of Electrical Power Engineering, University of Ruse, 8 Studentska Str., 7004 Ruse, Bulgaria; stoyanov@uni-ruse.bg
[5] Faculty of Electrical, Mechanical and Industrial Engineering, Anhalt University for Applied Sciences, 06366 Köthen, Germany; eduard.siemens@hs-anhalt.de
* Correspondence: tiliev@uni-ruse.bg

Abstract: The increasing frequency of wind turbine failures due to extreme weather conditions necessitates the implementation of new solutions to enhance their operational reliability. This paper presents an automatic rotor drop system specifically designed for wind turbines equipped with the Onipko rotor. The system aims to protect turbines from damage caused by critical wind speeds, reducing maintenance costs and extending the equipment's lifespan. The unique design of the Onipko rotor allows it to operate at wind speeds as low as 0.1 m/s. However, its high drag coefficient and lack of aerodynamic optimization make it susceptible to mechanical stress and structural instability under strong gusts, requiring additional protective measures. The paper presents a calculation of the critical wind speed at which protective measures must be initiated. Through mathematical modeling, this study demonstrates the effectiveness of the rotor drop system in ensuring safe operation at wind speeds reaching 23.5 m/s. The optimization of the PI controller parameters provides a rapid response and stability, significantly enhancing the resilience of wind turbines to adverse weather conditions.

Keywords: operational reliability; failure frequency; critical wind speed; Onipko rotor; automatic system; PI controller optimization

check for updates

Citation: Fazylova, A.; Iliev, T.; Stoyanov, I.; Siemens, E. Height Control System for Wind Turbines Based on Critical Wind Speed Calculation. *Appl. Sci.* **2024**, *14*, 9802. https://doi.org/10.3390/app14219802

Academic Editor: José António Correia

Received: 19 September 2024
Revised: 21 October 2024
Accepted: 25 October 2024
Published: 27 October 2024

Copyright: © 2024 by the authors. Licensee MDPI, Basel, Switzerland. This article is an open access article distributed under the terms and conditions of the Creative Commons Attribution (CC BY) license (https://creativecommons.org/licenses/by/4.0/).

1. Introduction

The steady demand for electrical energy in the world and environmental issues in that regard, especially the transition to fossil-free energy production, demand the active development of renewable energy production systems. Hereby, wind turbines play a key role in this process, providing fossil-free energy production. However, with the increasing number of wind turbines deployed in the field, the frequency of turbine failures due to strong wind gusts has also increased significantly [1]. One of the widely used control strategies in wind turbine management is the Proportional–Integral–Derivative (PID) controller. PID control technology has been a cornerstone in industrial automation for many decades due to its simplicity, reliability, and ease of implementation [2]. Despite its prevalence, the performance of PID controllers in highly dynamic environments like wind turbines can be limited [3]. These limitations arise due to the inherent delay and overshoot that PID controllers may experience under fast-changing wind conditions, leading to less precise control during gusty or turbulent events. Nonetheless, the continued use of PID control in wind turbine applications, including the Onipko rotor system, is driven by its low computational requirements and ease of tuning, which make it a cost-effective solution for many installations. This advantage is especially significant in resource-constrained

environments where more advanced controllers, such as Model Predictive Control (MPC), could introduce prohibitive costs in terms of both hardware and skilled personnel [4].

The introduction of new rotor models and technological advancements, while aimed at improving efficiency, has inadvertently heightened the risks associated with extreme weather conditions [5]. These risks include structural failures and increased maintenance costs due to the susceptibility of sophisticated components to damage under severe wind stress. Specifically, the vertical axis and lightweight design of the Onipko rotor contribute to uneven load distribution during high wind conditions, resulting in increased oscillations and potential rotor displacement, which can cause damage to the support structure and the main shaft bearings. To address these challenges, advanced control systems have been developed to ensure the safe and reliable operation of wind turbines during high wind events. In the context of the Onipko rotor, the use of a PID controller remains a practical choice due to its ability to provide reliable, albeit less sophisticated, control in managing rotor position and reducing mechanical stress. While more advanced control techniques offer superior performance in certain conditions, the robustness and simplicity of PID control make it suitable for managing the balance between cost and performance [6]. Despite these solutions, limitations in structural design remain, such as the lack of flexibility in the rotor blades, making them vulnerable to fatigue and possible detachment under extreme wind pressure. Implementing these control solutions helps to manage loads on turbine structures, minimize damage, and reduce the number of failures in extreme conditions. A study conducted in [7] shows that wind turbine blades are particularly susceptible to damage due to variable loads, especially under strong wind conditions. For example, the frequency of cracks at the blade tips is 77.78%, and in the middle parts of the blades, it is 22.22% [8]. Furthermore, an analysis of wind turbine equipment revealed that harsh operating conditions and long operational cycles significantly affect the reliability and maintenance costs of wind turbines [9]. To reduce the number of failures and increase the resilience of wind turbines to extreme weather conditions, new materials and technologies are being developed, such as advanced composite materials and active load control systems [10]. In this paper, we proposed a rotor-lowering control system as an effective method to address these issues, specifically enhancing the safety and operational stability of the Onipko rotor turbine in extreme wind conditions.

2. Related Work and State of the Art

Research in the field of automatic control systems and the optimization of wind turbine operations is currently actively developing, as evidenced by numerous publications in scientific journals. Below are the reviews of the most significant work, highlighting their achievements, limitations, and useful aspects for this study.

Vertical-axis wind turbines (VAWTs) encounter challenges such as turbulent wind flows near the ground, leading to inconsistent wind speeds and fluctuating loads on the blades. The Onipko rotor, as a vertical-axis wind turbine, requires specific control strategies to manage its unique structural dynamics under varying wind conditions. They also face cyclic loading due to the blades experiencing different wind conditions during rotation, causing material fatigue. To address these issues, Model Predictive Control (MPC) has been proposed for power regulation and turbine positioning. This control system ensures good performance and structural stability by directly controlling the tilt angle, blade pitch angle, and generator torque [11]. Simulations based on OpenFAST and Simulink have shown MPC's superiority over traditional PID controllers in some aspects, such as increased control accuracy and reliability. However, implementing MPC comes with significant challenges compared to PID controllers. MPC requires more complex algorithms, higher computational resources, and more sophisticated tuning processes, which can be difficult to implement in practical applications [12]. Moreover, these systems result in significantly higher capital and operational costs. Capital costs arise from the need for advanced computational infrastructure and hardware capable of supporting the high demands of real-time processing. Additionally, operational costs are driven by the continuous need

for maintenance and skilled personnel to handle the complexity of MPC algorithms [13]. On the other hand, PID controllers provide a more practical and economically feasible solution, especially for resource-constrained environments. Their ease of implementation, lower computational requirements, and minimal need for complex tuning make PID controllers an attractive choice for many wind turbine applications, including systems like the Onipko rotor. While MPC can provide superior performance in specific cases, PID controllers have proven to offer a reliable and cost-effective solution, particularly when long-term economic impacts such as the total cost of ownership, scalability, and operational reliability are considered [14]. On the other hand, traditional PID controllers have significant advantages, including ease of implementation, lower computational resource requirements, and straightforward tuning. This makes PID controllers a practical and cost-effective solution for many applications, including controlling the Onipko rotor during strong wind events, ensuring system reliability, and reducing the risk of component failure. PID controllers have proven themselves in the industry due to their reliability and effectiveness under a wide range of conditions [15]. Their simplicity allows for easy system integration and maintenance, making them a more practical and cost-effective solution for many applications than an MPC system.

The article published in [16] addresses the challenges of ensuring reliability, safety, and efficiency in wind turbine control. While advanced methods like adaptive and predictive control can optimize performance and reduce maintenance costs, they demand significant computational power. This computing power is crucial because it enables the real-time processing of complex algorithms, ensuring timely responses to changing conditions. However, the high computational requirements, along with the need for substantial initial investments and skilled personnel, can limit the practical application of these advanced methods, especially in resource-constrained environments.

The study published in [17] focuses on control strategies for wind turbine components using sensor-based systems. It highlights that integrating advanced monitoring and control technologies can enhance turbine stability and reduce the risk of failure under variable weather conditions. These technologies include using sensorless control methods to minimize hardware costs and employing real-time data processing techniques to detect and respond to load changes in turbine components.

The study published in [18] focuses on control strategies for vertical-axis wind turbines (VAWTs) and highlights the impact of active control systems on enhancing turbine efficiency. Implementing adaptive control techniques allows for real-time adjustments to varying wind conditions, which is crucial for improving the overall system performance and reliability. Such approaches are particularly beneficial for VAWTs like the Onipko rotor, as they reduce structural stress and improve the lifespan of key components [19]. This research demonstrates that optimizing control strategies rather than relying on purely aerodynamic design changes can be more effective in improving turbine efficiency and operational stability.

The sensorless wind speed and rotor position control method presented in [20] reduces hardware costs and increases system reliability. By eliminating the need for additional physical sensors to measure wind speed and rotor position, this method decreases the overall cost of the turbine system. Instead, it relies on the output data from the rotor current controller and uses machine learning methods, such as particle swarm optimization and support vector regression, to estimate these parameters. This approach not only reduces the number of components needed but also minimizes maintenance and potential points of failure, thereby enhancing the system's reliability.

The maximum power point tracking (MPPT) method improves energy conversion efficiency and reduces mechanical damage to wind turbines [21]. The study uses Fokker–Planck–Kolmogorov equations and the least squares method for the accurate tracking of the rotor speed probability density function shape, increasing power capture and reducing the frequency of system variable oscillations.

While MPPT can significantly enhance wind turbine efficiency by optimizing power output, its application comes with certain limitations. The complex algorithms involved require high computational resources and powerful hardware, which increase system costs and complicate setup. Unlike MPPT, PID controllers are simple to implement, do not demand extensive computational power, and easily integrate into various systems. This simplicity makes PID controllers a more preferred choice in situations where reliability, cost-effectiveness, and ease of use are crucial [22].

These studies highlight the critical importance of integrating advanced technologies and control methods to enhance the efficiency and reliability of wind turbines. This paper presents a control method that effectively addresses challenges such as high computational demands and the complexity of mathematical models. Unlike other approaches that require significant resources for data processing and complex algorithms, the proposed method leverages simpler yet highly effective algorithms that maintain a high level of system performance. This approach allows for the implementation of solutions in resource-constrained environments while ensuring the reliability and stability of the system's operation.

3. Proposed Materials and Methods

For the development of a linear actuator control system designed to lower the wind turbine during strong winds proposed in our research, various components were analyzed and investigated. This section provides a detailed description of the PID controller in use, the rationale for selecting the target values for the controller, a description of the chosen linear actuator, its mathematical model, and the details of the system integration, including sensors and the frequency converter. A PID controller is used to control a system with feedback, allowing the desired output value to be achieved by minimizing the error between the setpoint (SP) and the current process variable [23,24]. The block diagram of the wind turbines with a PI controller is shown in Figure 1.

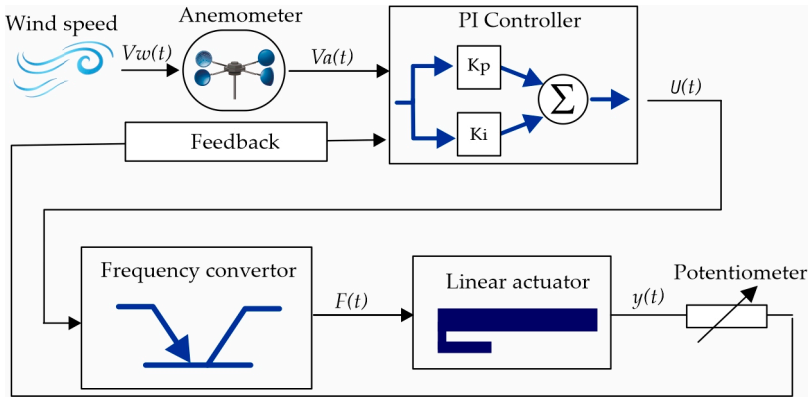


Figure 1. Schematic of the wind turbine height control system.

Figure 1 illustrates the automatic control system used to lower the rotor of the Onipko wind turbine under strong wind conditions. The system includes the following components:

- Anemometer: Measures wind speed $V_w(t)$ and outputs a corresponding voltage signal $V_a(t)$.
- PI Controller: Takes the anemometer's output as input and calculates the control signal $U(t)$ based on the error between the setpoint and the measured position. The PI controller uses proportional (K_p) and integral (K_i) gains to optimize the control signal.
- Frequency Converter: Converts the control signal $U(t)$ into an output frequency $F(t)$ to control the speed of the linear actuator.
- Linear Actuator: Lowers the turbine's rotor based on the output frequency from the frequency converter, adjusting its position $y(t)$.
- Potentiometer: Measures the current position of the rotor and feeds this value back to the controller to ensure accurate adjustment.

The closed-loop feedback mechanism ensures safe and precise operation, protecting the turbine from mechanical damage during high wind speeds by lowering the rotor to a safer position.

The diagram shown in Figure 2 represents an automatic control system using a PID controller to lower the wind turbine rotor during strong winds. The wind speed sensor (anemometer) measures the current wind speed and activates the control system if the wind speed exceeds a set threshold value. The setpoint is chosen as 40% of the full actuator stroke, determined based on the safety and efficiency requirements of the system. The difference between this set value and the current actuator position ($e = r - y$) is fed into the PI controller, which consists of proportional (KP) and integral (KI) components. These components adjust the control signal (u) proportionally to the current error, the accumulated error, and the rate of change in the error, respectively. The sum of these outputs forms the control signal that acts on the linear actuator, lowering the wind turbine rotor.

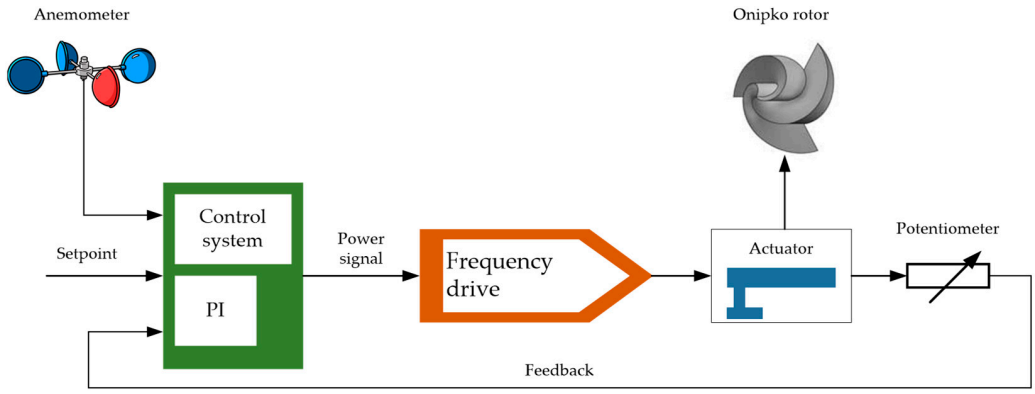


Figure 2. General PI controller-based control scheme.

A linear potentiometer installed on the actuator measures the current position of the actuator and feeds this information back into the system as feedback (linear displacement). In strong winds, the controller generates a control signal that activates the linear actuator to lower the rotor, reducing its rotational speed to a safe level, and ensuring the stable and safe operation of the wind turbine. The setpoint value of 40% is chosen to balance safety and efficiency: it sufficiently reduces the wind impact on the wind turbine when wind speed exceeds the threshold without requiring a complete lowering of the structure.

The Onipko rotor wind turbine was selected as the focus of this study due to its unique design, which, while highly efficient at low wind speeds, presents particular vulnerabilities to strong winds and uneven load distribution. These characteristics make it an ideal candidate for testing the rotor-lowering system, which aims to protect the rotor from damage during high wind events by reducing mechanical stress on the system [25].

Specifically, the Onipko rotor chosen for this study has the following characteristics [26]: a rotor diameter of 2 m, corresponding to a radius of 1 m. The air density through which the rotor operates is 1.225 kg/m^3, and the rotor's drag coefficient is 1. The associated generator is capable of producing up to 10 kW of power. The turbine is designed to operate at wind speeds ranging from 0.1 to 5.6 m/s, which encompasses the wind conditions found across much of the Earth's surface. Additionally, the rotor's spiral design creates an air cushion around it, significantly increasing its operational efficiency. These parameters, as detailed in previous research, provide a solid foundation for exploring and optimizing the rotor-lowering system in this study.

To configure the control system for optimal parameters, it is necessary to determine the critical wind speed. The critical wind speed is the threshold speed at which the wind turbine may be damaged or operate unstably due to excessive loads. An energy approach

has been used to calculate the critical wind speed value. The wind power P_{wind} can be expressed through the kinetic energy of the airflow [27]:

$$P_{wind} = \frac{1}{2}\rho A\vartheta^3, \quad (1)$$

where A is the cross-sectional area of the rotor; ρ is the air density; and ϑ is the wind speed.

The generator power P_{gen} is related to the wind power through the power utilization coefficient C_p, which can be calculated by the following [27]:

$$P_{gen} = C_p P_{wind}, \quad (2)$$

The wind force F can be represented by the following [28]:

$$F = \frac{1}{2}p\vartheta^2 AC_d \quad (3)$$

Based on the energy approach and the characteristics of the wind turbine, calculations were performed to determine the critical wind force and speed (see Table 1). Given the generator power of 10 kW and the power utilization coefficient $C_p \approx 0.4$, the wind power incident on the rotor is 25 kW. For this wind power, the calculated wind speed is approximately 23.5 m/s. At this speed, the wind force acting on the rotor is approximately 1058.65 N. Therefore, the critical wind force at which the rotor-lowering system should be activated is around 1058.65 N, which is close to the required value of 1200 N, considering errors and additional factors. This confirms that the target critical wind speed of around 25 m/s corresponds to the specified parameters of the wind turbine protection system.

Table 1. Calculation of the wind force and speed optimal for the studied wind turbine.

P_{wind}, kW	A, m^2	P_{gen}, kW	v, m/s	F, N
25	3.14	10	23.5	1058.65

4. Mathematical Model of the Control System

This section presents the mathematical model of the control system based on the interaction of the various components such as the anemometer, PI controller, frequency converter, and linear actuator. Each of these components is described by differential equations, allowing the creation of a comprehensive system model to ensure effective process control.

The anemometer is used to measure wind speed and transmit these data to the control system. It plays a crucial role because without accurate wind speed measurement, proper system control is impossible. The mathematical model of the anemometer is represented by a first-order linear differential equation [29]:

$$\tau_a \frac{dV_a(t)}{dt} + V_a(t) = K_a V_w(t), \quad (4)$$

where τ_a = 0.1 s—the time constant of the anemometer; $V_a(t)$ is the output voltage of the anemometer at a given moment in time t; K_a = 2 V/(m/s) is the conversion coefficient of wind speed to voltage; and $V_w(t)$—the wind speed at a given moment in time t.

Next, the Laplace transform of the equation was performed:

$$\tau_a s V_a(s) + V_a(s) = K_a V_w(s) \quad (5)$$

Solving Equation (10) for $V_a(s)$, the following was obtained:

$$V_a(S) = \frac{K_a}{\tau_a S + 1} V_w(s) \quad (6)$$

The inverse Laplace transform provides the solution in the time domain:

$$V_a(t) = K_a V_w(t)\left(1 - {}^{-t/\tau_a}\right) \tag{7}$$

The controller implementing the PI regulator adjusts the control signal based on the regulation error. The PI regulator combines proportional and integral actions to achieve optimal control. In the Laplace domain, the equation of the PI regulator is as follows [30]:

$$\bigcup(s) = k_P E(s) + \frac{k_i}{s} E(s), \tag{8}$$

where k_p is the proportional gain; k_i is the integral gain; and $E(s)$ is the regulation error in the Laplace domain.

$$E(s) = R(s) - Y(s), \tag{9}$$

where $R(s)$ is the setpoint and $Y(s)$ is the system output.

In the time domain, the equation of the PI regulator is as follows [31]:

$$u(t) = k_P e(t) + k_i \int_0^t (\tau) d\tau, \tag{10}$$

where $u(t)$ is the control signal at a given moment in time t and $e(t)$ is the regulation error.

$$e(t) = r(t) - y(t), \tag{11}$$

where $r(t)$ is the setpoint and $y(t)$ is the system output.

The frequency converter controls the frequency and, consequently, the speed of the linear actuator. It allows the precise control of the actuator's movement, ensuring smooth and accurate operation. The model of the frequency converter is described by the following differential equation:

$$\tau_f \frac{dF(t)}{dt} + F(t) = K_f U(t), \tag{12}$$

where τ_f = 0.2 s is the time constant of the frequency converter; $F(t)$ is the output frequency of the converter at a given moment in time t; K_f = 50 Hz/V is the conversion coefficient of voltage to frequency; and $U(t)$—the control voltage from the controller at a given moment in time t.

After applying the Laplace transform, the equation obtained is as follows:

$$\tau_f s F(s) + F(s) = k_f U(s) \tag{13}$$

Solving for $F(s)$:

$$F(s) = \frac{K_f}{\tau_f s + 1} U(s) \tag{14}$$

The inverse Laplace transform provides the solution in the time domain:

$$F(t) = K_f U(t)\left(1 - e^{-t/\tau_f}\right) \tag{15}$$

The linear actuator is responsible for the physical movement of the wind turbine rotor, adjusting its position based on wind speed to prevent damage and optimize operation. The dynamics of the linear actuator are described by the following second-order differential equation [32]:

$$m\frac{d^2y}{dt^2} + \mathrm{c}\frac{dy}{dt} + ky = F(t), \tag{16}$$

where m = 10 kg is the mass of the actuator; c = 50 Nm/c is the damping coefficient; k = 200 N/m is the spring stiffness; $y(t)$ is the displacement of the actuator at a given moment in time t; and $F(t)$ is the force applied to the actuator at a given moment in time t.

The Laplace transform of (21) is as follows:

$$ms^2Y(s) + csY(s) + kY(s) = F(s) \tag{17}$$

Solving for $Y(s)$, the equation obtained is as follows:

$$Y(s) = \frac{F(s)}{ms^2 + cs + k} \tag{18}$$

The inverse Laplace transform provides the solution in the time domain [33]:

$$y(t) = \mathcal{L}^{-1}\left\{\frac{F(s)}{ms^2 + cs + k}\right\} \tag{19}$$

A potentiometer is used to measure the current position of the linear actuator and provide feedback to the control system. The model of the potentiometer is described by the following linear equation [34]:

$$V_p(t) = K_v y(t), \tag{20}$$

where $V_p(t)$—the output voltage of the potentiometer at a given moment in time t; K_v = 0.5 V/m is the conversion coefficient of displacement to voltage; and $y(t)$ is the displacement of the linear actuator at a given moment in time t.

The connections between components through their output and input parameters should be considered to create a complete model of the control system. The wind speed $V_w(t)$ is measured by the anemometer, which converts it into the output voltage $V_a(t)$. This voltage is fed to the PI controller, which calculates the control signal $U(t)$ based on the regulation error $E(t)$. The control voltage $U(t)$ is applied to the frequency converter, which changes the frequency $F(t)$ according to the input signal. The frequency determines the force applied to the linear actuator. The linear actuator, in turn, moves the rotor by a distance $y(t)$, which is measured by the potentiometer. The potentiometer converts the displacement into an output voltage $V_p(t)$, which is fed back to the controller to adjust the control signal based on the current rotor position, thereby ensuring a closed control loop. By combining the mathematical model equations of each component, the complete system equation was obtained:

$$Y(s) = \frac{k_f\left(k_v(R(s) - Y(s)) + \frac{k_i}{s}(R(s) - Y(s))\right)}{\left(\tau_f s + 1\right)(ms^2 + cs + k)} \tag{21}$$

The presented mathematical model of the wind turbine control system demonstrates the importance of accurate measurement and proper parameter control to ensure the system's efficient operation and safety. Modeling the interactions between the anemometer, PI controller, frequency converter, and linear actuator allows for the precise adjustment and control of the process. Integrating all the components into a single system with a closed-loop control ensures the stable and reliable operation of the wind turbine, minimizing the risk of damage and optimizing performance.

5. Experimental Tuning of PI Controller Parameters

In this study, a detailed selection of PI controller coefficients was conducted for the rotor-lowering system of the Onipko wind turbine in strong wind conditions. The primary goal of the experiment was to determine the optimal values of the proportional (K_p), integral (T_i), and differential (T_d) coefficients to ensure reliable and stable system operation under high wind speeds. The PID controller cont_c in the TIA PORTAL software environment served as the object of the study. In the initial experiment, only the integral component was included, with an integration time of 20 s, a polling cycle time of 1 s, and a proportionality coefficient of 1. The response of the control signal LMN to the change in integration

time was analyzed with SP_INT = 40 and GAIN = 1. The results of the investigation are presented in Table 2.

Table 2. Study of the integral regulator.

T_i (ms)	Peak Value LMN	Transition Time (s)	Damping Coefficient (ψ)
10	90	-	1
50	90	27	0.25
80	73	26	0.15
100	67	23	0.14
110	66	23	0.09
200	52	22	0.08
300	42	23	≈0
500	40.9	21	≈0
1000	39.9	46	=0

In Figures 3–8 the red line (LMN_I) is the value of the integral component of the regulator (I-component), the white line (LMN) indicates the overall control signal of the system (LMN), the yellow line (ER) is a regulation error (Error, ER) and the green line is the desired value.

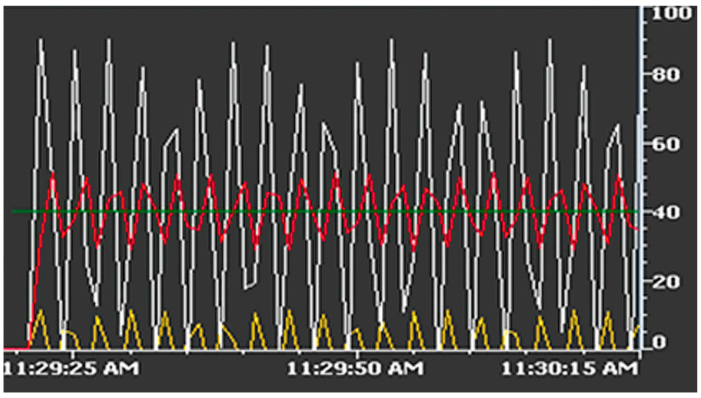


Figure 3. Integral regulator at T_i = 10 ms.

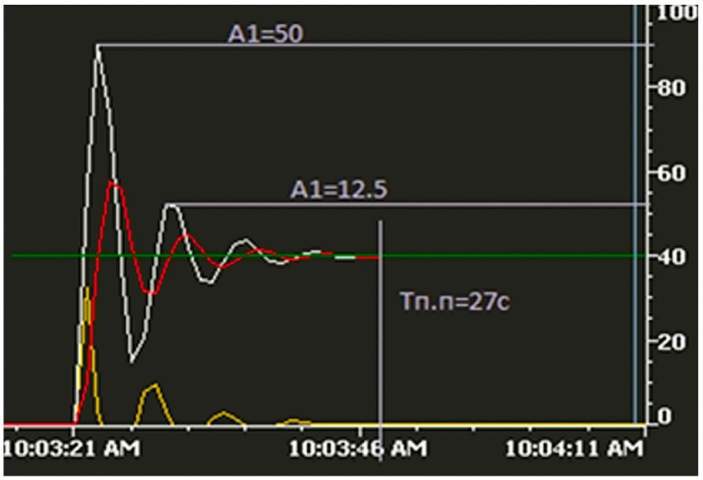


Figure 4. Integral regulator at T_i = 50 ms.

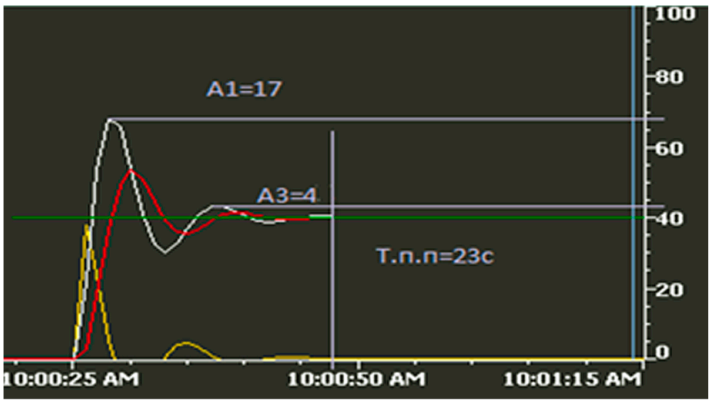


Figure 5. Integral regulator at T_i = 100 ms.

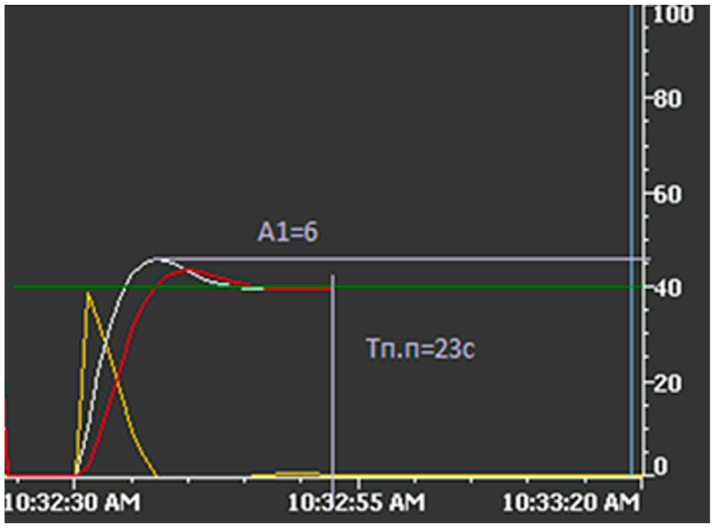


Figure 6. Integral regulator at T_i = 300 ms.

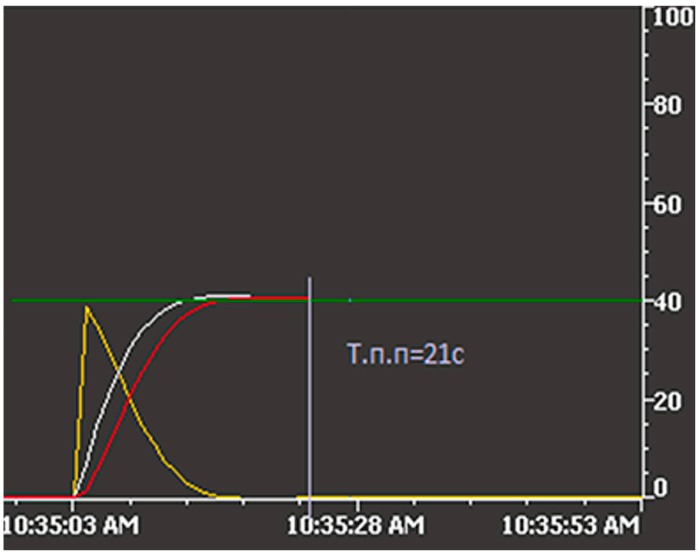


Figure 7. Integral regulator at T_i = 500 ms.

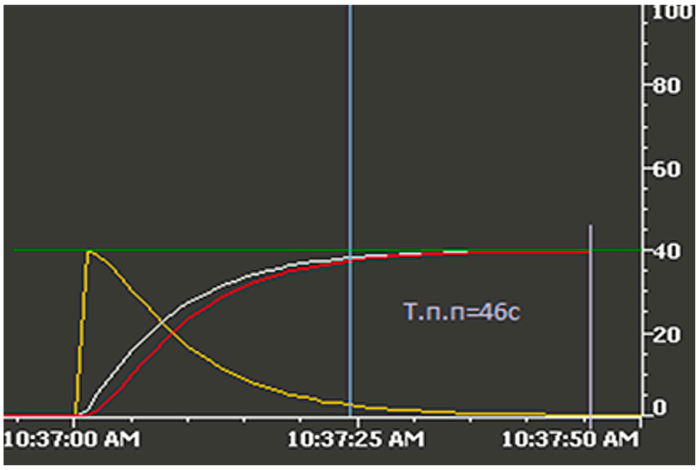


Figure 8. Integral regulator at T_i = 1000 ms.

The first integration time value was chosen to be 10 ms, during which the control signal entered self-oscillation and did not recover (Figure 3). At the minimum integration time T_i = 10 ms, persistent self-oscillations can be observed.

Increasing T_i to 50 ms provides an excellent control signal graph with damped oscillations (Figure 4), and the signal tends toward the desired value. The lines are the same as in Figure 3.

Gradually increasing the integration time led to a reduction in oscillations and an acceleration of the transition process (Figures 5 and 6). At T_i = 300 and 500 ms, the oscillations were so minimal that calculating the damping coefficient became impossible (Figures 7 and 8).

It should be noted that at T_i = 1000 ms, oscillations do not occur at all, and the control signal gradually approaches SP_INT exponentially. However, while previously the transition time gradually decreased with an increase in T_i, it has now doubled.

During the investigation of the P component, it was noted that as K_p increases, the value of the control signal gradually increases both at the beginning and the end of the transition process (Figures 9 and 10). Additionally, there is a trend of decreasing transition time. However, with very high values of K_p, for example, 10, the transition process destabilizes. The results are presented in Table 3.

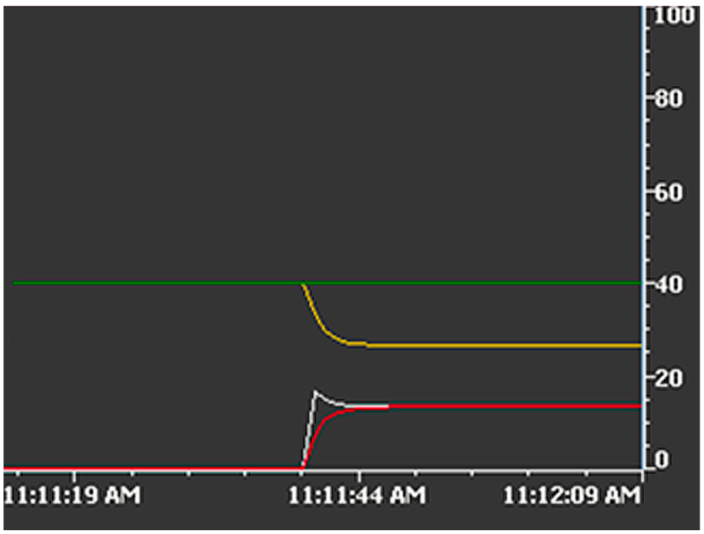


Figure 9. Proportional regulator at K_p = 0.5.

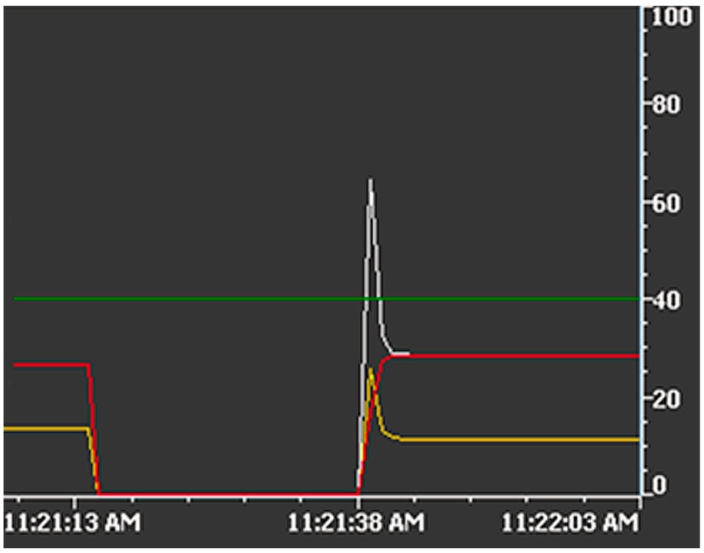


Figure 10. Proportional regulator at K_p = 2.5.

Table 3. Study of the proportional regulator.

Kp	Peak Value LMN	Steady State Value LMN	Transition Time (s)
0.5	17.9	13.3	≈7.5
1	33.6	20	≈6
1.5	60	24	≈6
2	75.7	26.6	≈5
2.5	64.3	28.6	≈5
5	120.4	33.3	≈2.5
10	333.3	36.4	≈4

In Figure 9 to Figure 10, the green line (SP_INT) represents the setpoint, the desired value the system aims to reach; the red line (PV_IN) is the current value of the controlled parameter (Process Variable); the yellow line (LMN_OBJECT) is the control signal generated by the PID regulator to reach the setpoint (SP_INT); and white line (LMN) the overall control signal of the system.

The next step involves combining the P and I components. The proportional gain was chosen to be 2.5 because at this value, the P component does not exceed the desired setpoint (SP_INT). The following results were obtained when varying the integration time, as shown in Table 4.

Table 4. Study of the PI regulator.

T_i (ms)	Integration Time (T_i)	Peak Value LMN	Transition Time (s)
10	93	≈30	Oscillatory
50	59	≈17	Oscillatory
100	45	≈13	Oscillatory
200	40	≈25	Exponential
500	40	≈65	Exponential

At small values of T_i, the control signal at the beginning of the transition process exhibits a distinctly oscillatory nature (Figure 11). The *I* component completely overshadows the *P* component due to its significantly larger magnitude. As the integration time increases further, the initial oscillations decrease (Figure 12), and subsequently, the transition process takes on an exponential form from the moment the influence of the *P* component ceases, but it takes significantly more time (Figure 13).

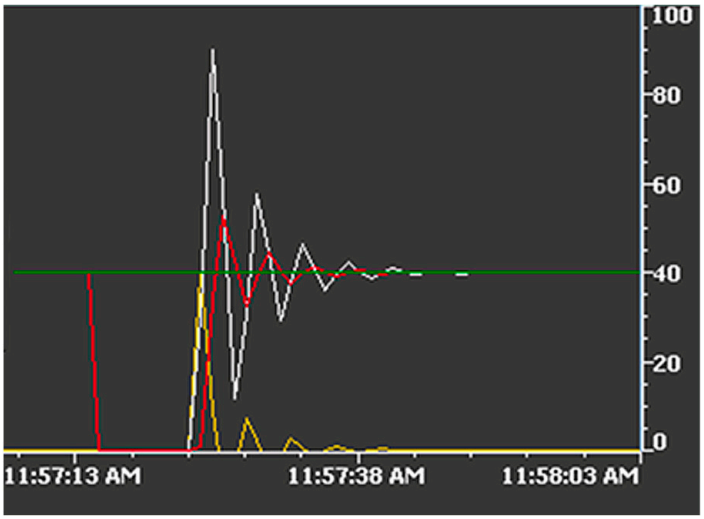


Figure 11. PI regulator at T_i = 10 ms.

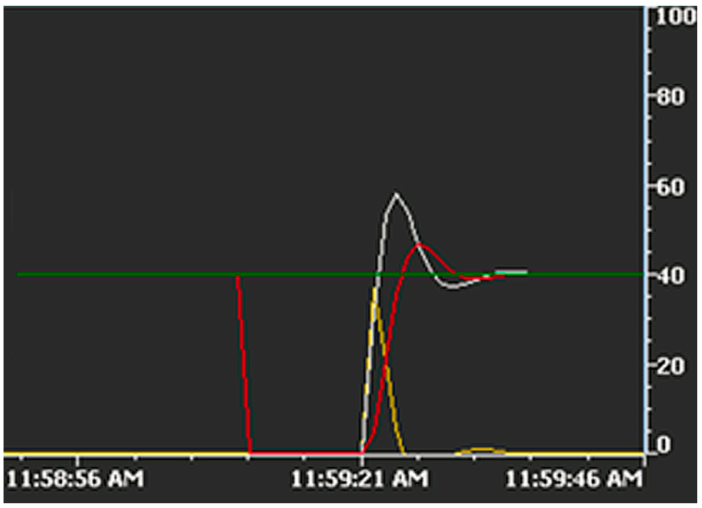


Figure 12. PI regulator at T_i = 50 ms.

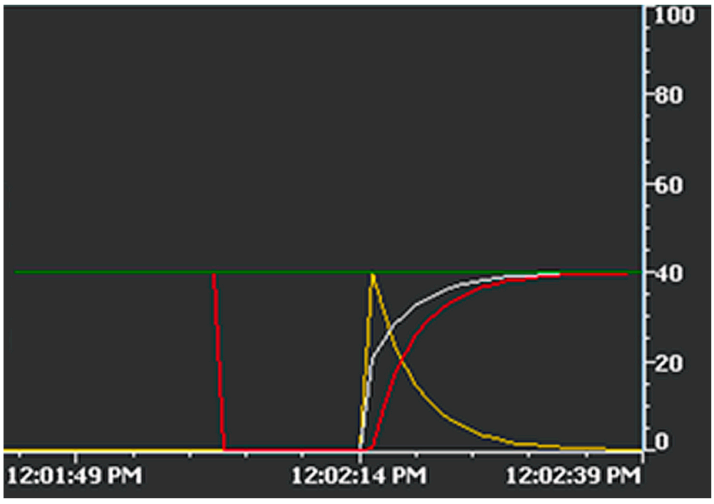


Figure 13. PI regulator at T_i = 200 ms.

In Figure 11 to Figure 13, the green line (SP_INT) is the setpoint (Set Point, SP_INT), the red line (PV_IN) is the current value of the controlled parameter (Process Variable, PV_IN), the yellow line (LMN_OBJECT) is the value of the control signal generated by the PID regulator to reach the setpoint (SP_INT), and white line (LMN) is the overall control signal of the system. In these figures, it shows the system's response.

The experimental results allowed for the determination of the optimal PI controller coefficients for the rotor-lowering system of the Onipko wind turbine in strong wind conditions. Based on the experimental data, the following parameters were chosen as optimal for the PI controller: a proportional coefficient K_p of 2.5 and an integration time T_i of 200 ms. These parameters provide an optimal balance between system stability and response speed, minimizing oscillations and ensuring a fast transition process. The accurate determination of these parameters significantly enhances the reliability and efficiency of the wind turbine rotor-lowering system at high wind speeds, preventing potential equipment damage and extending its lifespan. Thus, the system can operate effectively, minimizing the risk of accidents and ensuring stable electricity generation even in extreme weather conditions.

6. Results and Discussion

This chapter presents the results of the numerical calculation of the wind turbine control system based on the mathematical model described in Section 4. The model includes the interaction of the anemometer, PI controller, frequency converter, and linear actuator. Additionally, the experimentally obtained PI controller coefficients from Section 5 were used. For the complete control system model, the equation is as follows:

$$Y(s) = \frac{k_f\left(k_p(R(s) - Y(s)) + \frac{k_i}{s}(R(s) - Y(s))\right)}{\left(\tau_f s + 1\right)(ms^2 + cs + k)} \tag{22}$$

The following component parameters were used for substitution: k_f = Hz/V—conversion coefficient of voltage to frequency; k_p = 2.5—proportional coefficient of the PI controller; k_i = 5 s^{-1} (calculated as $k_i = \frac{1}{T_i}$ where T_i = 200 ms = 0.2, which corresponds to k_i = 5 s^{-1})—integral coefficient of the PI controller; τ_f= 0.2 s—time constant of the frequency converter; m = 10 kg—mass of the linear actuator; c = 50 Ns/m—damping coefficient; and k = 200 N/m—spring stiffness. Substituting these values into Equation (23), the following equation was obtained:

$$Y(s) = \frac{50\left(2.5(R(s) - Y(s)) + \frac{5}{s}(R(s) - Y(s))\right)}{(0.2s + 1)(10s^2 + 50s + 200)} \tag{23}$$

or

$$Y(s) = \frac{125R(s) + \frac{250R(s)}{s}}{(0.2s + 1)(10s^2 + 50s + 200)} - \frac{125Y(s) + \frac{250Y(s)}{s}}{(0.2s + 1)(10s^2 + 50s + 200)} \tag{24}$$

The code designed to perform numerical calculations for the wind turbine control system is given in (Appendix A Figure A1) and the flowchart is shown in Figure 14. It is based on the mathematical model described in Section 4 and incorporates the experimentally obtained PI controller coefficients from Section 5. The code performs numerical simulations, modeling the interaction of the system components: the anemometer, PI controller, frequency converter, and linear actuator. The output of the code is a graph showing the displacement of the linear actuator.

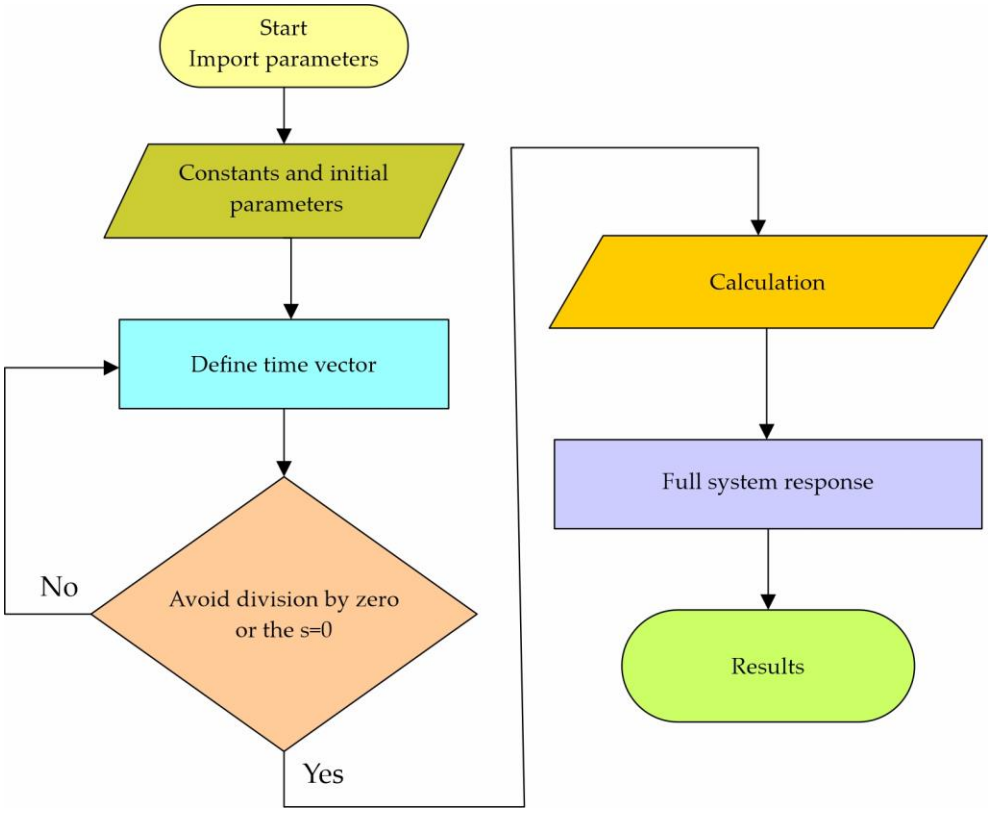


Figure 14. Flowchart of the mathematical model and the proposed program code.

The code defines the time vector and the Laplace variable. To prevent division by zero, the value of the Laplace variable at zero frequency is set to 1e-9. Then, the individual components of the system are calculated: the numerator of the equation, which includes the conversion of the signal to frequency (num_R), and the denominator of the equation, which includes the damping and stiffness effects of the system (denom). The complete system response in the frequency domain (Y_s) is calculated by dividing the numerator by the denominator, after which the inverse Laplace transform is performed to obtain the time-domain displacement of the actuator (y_t). Finally, the code plots the graph, showing the displacement of the linear actuator over time. The graph demonstrates the system's adequate response to changes in the wind speed, proper PI controller tuning, and correct damping, which is important to prevent sharp oscillations and system damage.

Figure 15 shows the displacement of the wind turbine's linear actuator.

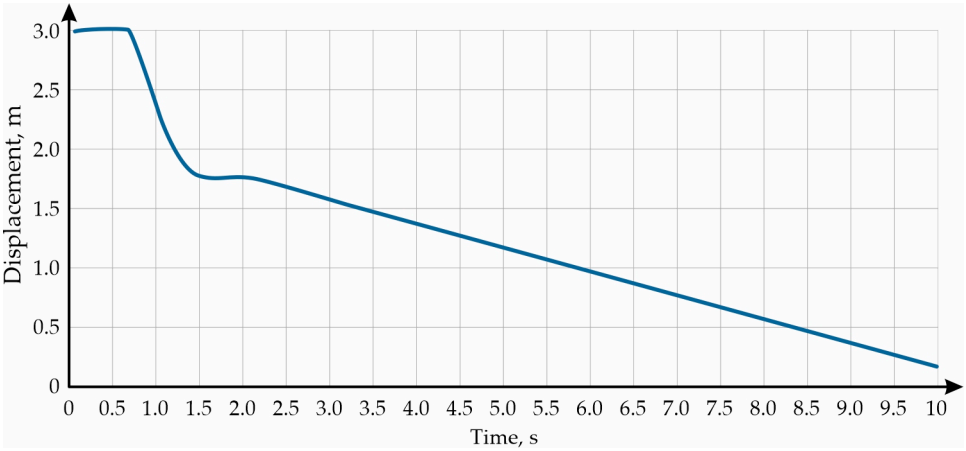


Figure 15. Wind turbine height control system.

The analysis of Figure 15 shows the displacement of the linear actuator, which is responsible for lowering the wind turbine rotor. At the start of the graph, there is a small delay before the actuator begins to move. This delay occurs because the system is analyzing the incoming data to decide when to activate the actuator. Once the system triggers, the graph displays a smooth and controlled lowering of the rotor, where the actuator moves down by 40% of its full stroke over a period of approximately 9 s.

This smooth and gradual motion demonstrates that the control system is operating correctly, avoiding sudden movements that could cause mechanical stress or instability. The key indication of the system's effectiveness is the absence of sharp oscillations, showing that the actuator's response is well damped and controlled. This confirms that the tuning of the PI controller parameters is optimal, allowing the actuator to move efficiently and precisely according to the specified control strategy. The overall result illustrated by the graph shows that the control system reliably performs the necessary adjustments to the rotor's position. This ability to smoothly lower the rotor ensures the safety and stability of the entire turbine structure, reducing the risk of potential mechanical damage and contributing to the longevity and reliability of the wind turbine.

7. Conclusions

The developed automatic rotor-lowering system for wind turbines has demonstrated its effectiveness when the critical wind speed of 23.5 m/s is reached, contributing to the reduction in operational costs and the extension of equipment lifespan. This critical wind speed value was mathematically calculated, and the effectiveness of the system was validated through experimental testing, where the system successfully lowered the rotor in under 9 s, as shown in Figure 15. The system enhances the reliability and durability of wind turbines, ensuring their ability to withstand extreme weather conditions without significant damage. The experimental results indicated that the optimized PI controller parameters, such as a proportional gain of 2.5 and an integration time of 200 ms, significantly minimized oscillations during rotor lowering. The precise tuning of these parameters allowed for the smooth and safe lowering of the rotor, preventing sharp oscillations that could damage the system. Furthermore, although the developed control system is specifically designed for the Onipko rotor, the proposed methodology and algorithms can be adapted for other types of rotors. This flexibility allows the system to be implemented in various wind turbine configurations where similar protection mechanisms are required. Additional research is recommended to validate the application of this system to different rotor designs, ensuring optimal performance and stability under extreme wind conditions. The system's ability to operate efficiently under various wind conditions ensures continuous and stable energy production, which is vital for meeting growing energy demands. The reduction in maintenance and repair costs, as well as the increase in turbine lifespan, makes this system a valuable addition to wind energy infrastructure.

A key novel contribution of this study is its focus on providing a practical and cost-effective solution for resource-constrained environments. While many advanced control systems, such as Model Predictive Control (MPC), offer superior performance, they often require significant computational resources and complex hardware, making them less accessible for smaller wind energy installations. The simplicity and affordability of the PI controller-based approach presented in this work provide a viable alternative that can be easily implemented in diverse operational settings, including those with limited financial and technical resources. This balance between cost-effectiveness and performance makes the system applicable to a wider range of wind turbines, expanding its potential impact on the renewable energy sector.

Author Contributions: Conceptualization, A.F., T.I., I.S. and E.S.; methodology, A.F., T.I., I.S. and E.S.; software, A.F. and E.S.; validation, A.F., T.I. and E.S.; formal analysis, A.F., T.I., I.S. and E.S.; investigation, A.F., T.I. and E.S.; resources, A.F., T.I., I.S. and E.S.; data curation, A.F., T.I., I.S. and E.S.; writing—original draft preparation, A.F., T.I., I.S. and E.S.; writing—review and editing, A.F., T.I. and

E.S.; visualization, T.I., I.S. and E.S.; supervision, I.S., T.I. and A.F. All authors have read and agreed to the published version of the manuscript.

Funding: This study was financed by the European Union-Next Generation EU through the National Recovery and Resilience Plan of the Republic of Bulgaria, project No. BG-RRP-2.013-0001-C01.

Institutional Review Board Statement: Not applicable.

Informed Consent Statement: Not applicable.

Data Availability Statement: Data are contained within the article.

Acknowledgments: 1. This article is based on research conducted within the framework of the project "Development of a control and monitoring system for a multi-blade vertical-axis wind generator" of the Committee of Science of the Ministry of Science and Higher Education of the Republic of Kazakhstan (Grant No: AP19679162). 2. This research was supported by the German Academic Exchange Service (DAAD) under the Förderprogramm for German language study programs (Deutschsprachige Studiengänge, DSG) in Central, Eastern, and Southeastern Europe, the Caucasus, and Central Asia for the 2023/24 academic year, project number DAAD—57663389.

Conflicts of Interest: The authors declare no conflicts of interest.

Appendix A. Program Code for Numerical Calculations for the Wind Turbine Control System

```
      import numpy as np
      import matplotlib.pyplot as plt
      # Constants and initial parameters
      tau_a = 0.1  # time constant of anemometer in seconds
      K_a = 2  # conversion coefficient of wind speed to voltage in V/(m/s)
      tau_f = 0.2  # time constant of frequency converter in seconds
      K_f = 50  # conversion coefficient of voltage to frequency in Hz/V
      m = 10  # mass of the drive in kg
      c = 50  # damping coefficient in Ns/m
      k = 200  # spring stiffness in N/m
      K_p = 2.5  # proportional coefficient
      K_i = 5  # integral coefficient (inverse of integration time in seconds)
      R_s = 1  # Reference input in Laplace domain
      # Define time vector
      time = np.linspace(0, 10, 1000)  # time from 0 to 10 seconds
      s = 1j * 2 * np.fft.fftfreq(len(time), d=(time[1]-time[0]))  # Laplace
variable
      # Avoid division by zero for the s=0 case
      s[0] = 1e-9
      # Calculate each term separately
      num_R = K_f * (K_p + K_i / s) * R_s
      denom = (tau_f * s + 1) * (m * s**2 + c * s + k)
      # Full system response
      Y_s = num_R / denom
      y_t = np.fft.ifft(Y_s).real
      # Scale displacement to match the real system's range
      y_t = y_t * (3 / np.max(np.abs(y_t)))  # Scale to maximum 3 meters
      # Plot results
      plt.figure(figsize=(10, 6))
      plt.plot(time, y_t, label='Drive Displacement (m)')
      plt.xlabel('Time (s)')
      plt.ylabel('Displacement (m)')
      plt.title('Linear Drive Displacement (scaled to 3 meters)')
      plt.legend()
      plt.grid()
      plt.show()
```

Figure A1. Program code for numerical calculations for the wind turbine control system.

References

1. Wang, J.; Qin, S.; Jin, S.; Wu, J. Estimation methods review and analysis of offshore extreme wind speeds and wind energy resources. *Renew. Sustain. Energy Rev.* **2015**, *42*, 26–42. [CrossRef]
2. Park, J.; Kim, C.; Dinh, M.-C.; Park, M. Design of a Condition Monitoring System for Wind Turbines. *Energies* **2022**, *15*, 464. [CrossRef]

3. Ogata, K. *Modern Control Engineering*, 5th ed.; Prentice Hall: Upper Saddle River, NJ, USA, 2010; p. 904.
4. Costa, Á.M.; Orosa, J.A.; Vergara, D.; Fernández-Arias, P. New Tendencies in Wind Energy Operation and Maintenance. *Appl. Sci.* **2021**, *11*, 1386. [CrossRef]
5. Santelo, T.N.; de Oliveira, C.M.R.; Maciel, C.D.; Monteiro, J.R.B.d.A. Wind Turbine Failures Review and Trends. *J. Control Autom. Electr. Syst.* **2022**, *33*, 505–521. [CrossRef]
6. Stoyanov, I.; Iliev, T.; Fazylova, A.; Yestemessova, G. A Dinamic Control model of the blades position for the vertical-axis wind generator by a program method. *Inventions* **2023**, *8*, 120. [CrossRef]
7. Besnard, F.; Bertling, L. An approach for condition-based maintenance optimization applied to wind turbine blades. *IEEE Trans. Sustain. Energy* **2010**, *1*, 77–83. [CrossRef]
8. Fazylova, A.; Balbayev, G.; Ilieva, D.; Aliyarova, M. Analysis of rotors' critical mode of operation to be employed in the design of a wind generation control unit. *E3S Web Conf.* **2020**, *180*, 02001. [CrossRef]
9. Jung, C.; Schindler, D.; Buchholz, A.; Laible, J. Global Gust Climate Evaluation and Its Influence on Wind Turbines. *Energies* **2017**, *10*, 1474. [CrossRef]
10. Li, H.; Peng, W.; Huang, C.-G.; Guedes Soares, C. Failure Rate Assessment for Onshore and Floating Offshore Wind Turbines. *J. Mar. Sci. Eng.* **2022**, *10*, 1965. [CrossRef]
11. Ha, K.; Truong, H.V.A.; Dang, T.D.; Ahn, K.K. Recent Control Technologies for Floating Offshore Wind Energy System: A Review. *Int. J. Precis. Eng. Manuf.-Green Tech.* **2021**, *8*, 281–301. [CrossRef]
12. Cao, L.; Qian, Z.; Zareipour, H.; Huang, Z.; Zhang, F. Fault diagnosis of wind turbine gearbox based on deep bi-directional long short-term memory under time-varying non-stationary operating conditions. *IEEE Access* **2019**, *7*, 155219–155228. [CrossRef]
13. Liu, X.; Feng, L.; Kong, X. A Comparative Study of Robust MPC and Stochastic MPC of Wind Power Generation System. *Energies* **2022**, *15*, 4814. [CrossRef]
14. Bai, X.; Zhan, H.; Mi, B. A New Flow Control and Efficiency Enhancement Method for Horizontal Axis Wind Turbines Based on Segmented Prepositive Elliptical Wings. *Aerospace* **2023**, *10*, 796. [CrossRef]
15. Yin, X.; Zhang, W.; Jiang, Z.; Pan, L. Adaptive robust integral sliding mode pitch angle control of an electro-hydraulic servo pitch system for wind turbine. *J. Mech. Syst. Signal Process.* **2019**, *133*, 105704. [CrossRef]
16. Yin, X.-X.; Lin, Y.-G.; Li, W.; Gu, Y.-J. Integrated pitch control for wind turbine based on a novel pitch control system. *J. Renew. Sustain. Energy* **2014**, *6*, 043106. [CrossRef]
17. Jameel, S.S.; Raazi, S.M.K.R.; Jameel, S.M. Multimodal ML Strategies for Wind Turbine Condition Monitoring in Heterogeneous IoT Data Environments. In *Forthcoming Networks and Sustainability in the AIoT Era*; Rasheed, J., Abu-Mahfouz, A.M., Fahim, M., Eds.; Lecture Notes in Networks and Systems; Springer: Berlin/Heidelberg, Germany, 2024. [CrossRef]
18. Elkodama, A.; Ismaiel, A.; Abdellatif, A.; Shaaban, S.; Yoshida, S.; Rushdi, M.A. Control Methods for Horizontal Axis Wind Turbines (HAWT): State-of-the-Art Review. *Energies* **2023**, *16*, 6394. [CrossRef]
19. Mahmoud, M.S.; Oyedeji, M.O. Adaptive and predictive control strategies for wind turbine systems: A survey. *IEEE/CAA J. Autom. Sin.* **2019**, *6*, 364–378. [CrossRef]
20. Abo-Khalil, A.G.; Eltamaly, A.M.; PR, P.; Alghamdi, A.S.; Tlili, I. A Sensorless Wind Speed and Rotor Position Control of PMSG in Wind Power Generation Systems. *Sustainability* **2020**, *12*, 8481. [CrossRef]
21. Zhang, X.; Zhang, Z.; Jia, J.; Zheng, L. A Maximum Power Point Tracking Control Method Based on Rotor Speed PDF Shape for Wind Turbines. *Appl. Sci.* **2022**, *12*, 9108. [CrossRef]
22. Pande, J.; Nasikkar, P.; Kotecha, K.; Varadarajan, V. A Review of Maximum Power Point Tracking Algorithms for Wind Energy Conversion Systems. *J. Mar. Sci. Eng.* **2021**, *9*, 1187. [CrossRef]
23. Alipbayev, K.; Ivanov, K.; Sultan, A.; Komekbayev, A. Research and design of an efficient adaptive drive with balancing friction coupling. *J. Appl. Eng. Sci.* **2024**, *22*, 81–88. [CrossRef]
24. Zhu, H.; Sueyoshi, M.; Hu, C.; Yoshida, S. A study on a floating type shrouded wind turbine: Design, modeling and analysis. *Renew. Energy* **2019**, *134*, 1099–1113. [CrossRef]
25. Kim, K.C.; Ji, H.S.; Kim, Y.K.; Lu, Q.; Baek, J.H.; Mieremet, R. Experimental and Numerical Study of the Aerodynamic Characteristics of an Archimedes Spiral Wind Turbine Blade. *Energies* **2014**, *7*, 7893–7914. [CrossRef]
26. Kalmikov, A. Wind Power Fundamentals. Massachusetts Institute of Technology. Available online: http://web.mit.edu/wepa/WindPowerFundamentals.A.Kalmikov.2017.pdf (accessed on 12 June 2024).
27. Roibas-Millan, E.; Cubas, J.; Pindado, S. Studies on Cup Anemometer Performances Carried out at IDR/UPM Institute. Past and Present Research. *Energies* **2017**, *10*, 1860. [CrossRef]
28. Fazylova, A.; Tultayev, B.; Iliev, T.; Stoyanov, I.; Beloev, I. Development of a Control Unit for the Angle of Attack of a Vertically Axial Wind Turbine. *Energies* **2023**, *16*, 5202. [CrossRef]
29. Song, Y.; Wang, B. Survey on reliability of power electronic systems. *IEEE Trans. Power Electron.* **2013**, *28*, 591–604. [CrossRef]
30. Chou, J.S.; Chiu, C.K.; Huang, I.K.; Chi, K.N. Failure analysis of wind turbine blade under critical wind loads. *J. Eng. Fail. Anal.* **2013**, *27*, 99–118. [CrossRef]
31. Wang, Y.; Hu, W. Investigation of the effects of receptors on the lightning strike protection of wind turbine blades. *IEEE Trans. Electromagn. Compat.* **2017**, *59*, 1180–1187. [CrossRef]
32. Acho, L.; Buenestado, P.; Pujol, G. A Finite-Time Control Design for the Discrete-Time Chaotic Logistic Equations. *Actuators* **2024**, *13*, 295. [CrossRef]

33. Li, L.; Chopra, I.; Zhu, W.; Yu, M. Performance Analysis and Optimization of a Vertical-Axis Wind Turbine with a High Tip-Speed Ratio. *Energies* **2021**, *14*, 996. [CrossRef]
34. Bariša, T.; Sumina, D.; Pravica, L.; Čolović, I. Flying start and sensorless control of permanent magnet wind power generator using induced voltage measurement and phase-locked loop. *Electr. Power Syst. Res.* **2017**, *152*, 457–465. [CrossRef]

Disclaimer/Publisher's Note: The statements, opinions and data contained in all publications are solely those of the individual author(s) and contributor(s) and not of MDPI and/or the editor(s). MDPI and/or the editor(s) disclaim responsibility for any injury to people or property resulting from any ideas, methods, instructions or products referred to in the content.